Impacts of Urban Albedo Increase on Local Air Temperature at Daily–Annual Time Scales: Model Results and Synthesis of Previous Work

E. SCOTT KRAYENHOFF

Department of Geography, University of British Columbia, Vancouver, British Columbia, Canada

JAMES A. VOOGT

Department of Geography, University of Western Ontario, London, Ontario, Canada

(Manuscript received 28 July 2009, in final form 10 January 2010)

ABSTRACT

The authors combine urban and soil–vegetation surface parameterization schemes with one-dimensional (1D) boundary layer mixing and radiation parameterizations to estimate the maximum impact of increased surface albedo on urban air temperatures. The combined model is evaluated with measurements from an urban neighborhood in Basel, Switzerland, and the importance of surface–atmosphere model coupling is demonstrated. Impacts of extensive albedo increases in two Chicago, Illinois, neighborhoods are modeled. Clear-sky summertime reductions of diurnal maximum air temperature for the residential neighborhood ($\lambda_p = 0.33$) are −1.1°, −1.5°, and −3.6°C for uniform roof albedo increases of 0.19, 0.26, and 0.59, respectively; reductions are about 40% larger for the downtown core ($\lambda_p = 0.53$). Realistic impacts will be smaller because the 1D modeling approach ignores advection; a lake-breeze scenario is modeled and temperature reductions decline by 80%. Assuming no advection, the analysis is extended to seasonal and annual time scales in the residential neighborhood. Yearly average temperature decreases for a 0.59 roof albedo increase are about −1°C, with summer (winter) reductions about 60% larger (smaller). Annual cooling degree-day decreases are approximately offset by heating degree-day increases and the frequency of very hot days is reduced. Despite the variability of modeling approaches and scenarios in the literature, a consistent range of air temperature sensitivity to albedo is emerging; a 0.10 average increase in neighborhood albedo (a 0.40 roof albedo increase for $\lambda_p = 0.25$) generates a diurnal maximum air temperature reduction of approximately 0.5°C for ''ideal'' conditions, that is, a typical clear-sky midlatitude summer day.

1. Introduction

Surface modifications arising from urbanization result in a tendency for urban areas to exhibit elevated temperatures relative to their nonurbanized surroundings, a phenomenon often loosely termed ''the urban heat island.'' Urban heat islands impact urban residents in several ways (e.g., Oke 1997), including modified energy demand (higher in summer, lower in winter), thermal stress on inhabitants, and increased air pollution formation rates.

There is convincing evidence that heat more generally is the most deadly of all natural hazards faced in the United States (Borden and Cutter 2008). Moreover, heat waves are considered ''very likely'' to become ''more intense, more frequent and longer lasting'' under current global climate projections (Meehl et al. 2007). Recent well-documented examples of deadly heat waves include those of Chicago, Illinois, in 1995 and 1999 and Europe in 2003. Urban temperature depends on local-scale and microscale processes in addition to the larger-scale (e.g., synoptic) weather patterns that typically drive heat waves. Cities are logical sites for heat attenuation at these smaller scales through intentional surface modification, and because of their high population densities, they have become the foci of such efforts.

In this context, numerical models of urban surface-exchange processes have been applied to study neighborhood-scale (local scale) urban heat mitigation options (e.g., Sailor 1995; Taha et al. 1999; Krayenhoff et al. 2003; Synnefa et al. 2008). These are often referred to as heat *island* mitigation studies, but it is in fact absolute urban air temperature that is of relevance rather than its difference from a nearby ''rural'' site. The focus

Corresponding author address: Scott Krayenhoff, Department of Geography, University of British Columbia, 1984 West Mall, Vancouver, BC V6T 1Z2, Canada.
E-mail: skrayenh@gmail.com

DOI: 10.1175/2010JAMC2356.1

of these studies is usually the reduction of daytime or maximum diurnal temperature; in contrast, the canopy-layer urban heat island (i.e., the elevation of street-level air temperature relative to a nearby rural site) is typically best expressed during the evening and nighttime (Oke 1982). Hence, the motivation for urban heat mitigation strategies is considered here apart from the ''urban heat island'' framework. Such strategies simply take advantage of the concentrations within cities of relatively modifiable surfaces and especially of potential benefactors, that is, people and their associated energy use, comfort, and health outcomes.

In this research, we focus on the sensitivity of near-surface air temperature to changes in roof albedo in neighborhoods with different degrees of urbanization. We use a simple 1D modeling framework that parameterizes both the urban roughness sublayer and the boundary layer above, but ignores horizontal transport by wind (advection). The neglect of advection (i.e., the assumption of an ''infinite city'') enables the estimation of maximum impacts of albedo modification on temperature, as advection always serves to reduce these impacts. These impacts are estimated at daily, seasonal, and yearly time scales for a midlatitude city with distinct warm and cold seasons as well as a history of deadly heat waves (Chicago). We then compare our estimates of near-surface air temperature sensitivity to albedo with results from other modeling studies in the literature.

Degree-days are a simple measure of the cooling or heating energy expenditure required to maintain comfortable indoor temperature. Apart from Taha et al. (1999), most studies relating urban surface modification to local-scale thermal changes have focused on cities characterized by a relatively high ratio of cooling degree-days (CDD) to heating degree-days (HDD) (e.g., 1.6 for downtown Los Angeles, CA, 2.7 for Houston, TX, and 3.7 for Phoenix, AZ) and significant periods of elevated heat stress and/or air pollution episodes. Therefore, an additional question that we begin to address here is whether urban heat mitigation is relevant or even beneficial in midlatitude cities that experience distinctly cold winters (with more HDD) as well as hot summers.

A discussion of the modeling approach and its evaluation against observational data follows in sections 2 and 3. In section 4, the modeled sensitivity of canopy-layer temperature to roof albedo at several time scales is discussed, and a synthesis of results from similar studies is undertaken.

2. Model combination

A combination of models provides a simple but relatively complete description of the boundary layer and surface radiation, heat, moisture, and momentum exchanges. Here, we couple the Town Energy Balance (TEB) urban surface scheme of Masson (2000) with a column model—the atmospheric boundary layer (ABL) portion of the Oregon State University Coupled Atmosphere–Plant–Soil (OSU-CAPS) model to simulate the urban energy balance. The two models are coupled such that they run interactively at each time step and require little outside forcing. The coupled model output provides estimates of the urban surface radiation and energy balances and their impact on both the averaged canopy-layer atmosphere and the overlying atmospheric boundary layer.

a. TEB urban surface scheme

TEB provides a relatively complete description of the urban surface energetics occurring within the urban canopy layer for nonvegetated urban surfaces. TEB represents urban areas through the concept of the urban street canyon: the space between two buildings bordered by the street, two walls, and the sky above. The surface is divided into three surface types—roofs, streets, and walls—each with their own energy budget, thermal and radiative properties, and temperatures. Individual buildings are not resolved, but instead their average impact on the urban canopy and boundary layers is parameterized. The TEB model as used here includes the updates described in Masson et al. (2002) and Lemonsu et al. (2004).

b. OSU

The OSU-CAPS atmospheric boundary layer model (hereinafter OSU) parameterizes the one-dimensional (vertical) exchange of heat, moisture, and momentum in the boundary layer. It was originally formulated by Troen and Mahrt (1986), with developments by Holtslag et al. (1990) and Chang and Ek (1996), among others. Mechanical (local) generation of mixing and also buoyant (nonlocal) mixing are modeled. OSU uses a simple 1D K-profile parameterization of vertical mixing. The inclusion of a countergradient term accounts for nonlocal mixing during convective conditions. Mechanical mixing is driven by the input geostrophic wind speed and the momentum flux estimated by the surface scheme(s).

Subsidence is important for maintaining the capping inversion during convective conditions in OSU simulations; here an input profile (peak: -0.012 m s^{-1}near 2 km) is estimated and remains constant for all clear-sky simulations. We add the simple five-band longwave scheme of Roach and Slingo (1979, hereafter RS79) to account for longwave exchanges and longwave cooling–heating within the atmosphere, and a shortwave scheme based on the Bird and Hulstrom (1981) model,

as presented in Iqbal (1983), to more robustly parameterize the incoming direct and diffuse solar radiation at the urban surface. This latter model, while simple, demonstrates excellent performance relative to both observations and more complex models (e.g., Gueymard and Myers 2008).

c. Vegetation–atmosphere parameterization

The OSU-CAPS soil–vegetation scheme (Mahrt and Pan 1984; Pan and Mahrt 1987; Ek and Mahrt 1991) parameterizes surface–atmosphere and subsurface interactions for vegetated areas. It is run as a simple three-layer soil model with a single vegetation layer, and accounts for the thermodynamics and moisture dynamics of the soil and vegetation, most notably evapotranspiration and thermal and water storage. In urban simulations that include natural areas, it is assumed to absorb, reflect, and emit radiation as if it was on the canyon floor in TEB, but is otherwise treated independently from TEB (i.e., it is effectively another ''tile'' in terms of its interactions with OSU). For rural simulations, the soil–vegetation scheme provides the complete boundary conditions to OSU and does not interact with TEB.

d. Model coupling

Surface boundary conditions to the OSU boundary layer model are supplied by TEB and the soil–vegetation scheme for urban and natural areas, respectively. Both schemes require temperature, wind speed, and mixing ratio at the lowest OSU model level, in addition to longwave flux from RS79 and incident solar, as input. They output sensible heat, latent heat, and momentum fluxes to OSU, and longwave flux to RS79, weighted by the urban and natural fractions. OSU surface boundary conditions and hence eddy diffusivities are then dependent on weighted average surface scheme output fluxes and temperatures. As TEB is a dual source model (i.e., roofs and canyons interact independently with the modeled atmosphere), roof properties impact the canopy thermal environment solely via the boundary layer model. However, the consistently close correspondence of TEB canyon air temperature and OSU air temperature at the lowest model level (not shown) suggests that the model efficiently mixes rooftop influences to the canyon air. This is not surprising given the high roughness and strong daytime surface heating of the modeled scenarios.

e. Advection

Advection can be a large term in the energy balance, particularly where substantial horizontal gradients exist, for example near urban–rural or land–water boundaries. Rural–urban advection is estimated here to demonstrate the approximate magnitude of its effects; the parameterization that is used is not intended to provide realistic results for a specific scenario. A modeled rural boundary layer is assumed to provide a reasonable approximation of the atmospheric profile upstream of the city in any given direction. For advection from a water body, the upstream distance to the land–water boundary is chosen. A simple relaxation-type advection equation is used:

$$\frac{\partial T_{\mathrm{urb}}(z)}{\partial t} = U(z)\frac{[T_{\mathrm{rur}}(z) - T_{\mathrm{urb}}(z)]}{\Delta x}, \qquad (1)$$

where Δx is the distance from the urban site or neighborhood being modeled to the rural–urban boundaries or land–water boundary, and $T_{\mathrm{rur}}(z)$, $T_{\mathrm{urb}}(z)$, and $U(z)$ are the rural–water temperature, urban temperature, and wind speed, all at height z as calculated in the urban simulation. For an average daytime mixed layer wind speed of 4 m s^{-1}, this translates into a relaxation time $\tau = \Delta x/U(z)$ of approximately 12–13 min, which is somewhat larger than that chosen by Clark and Hopwood (2001) as a free atmosphere value. For rural–urban advection we assume internal boundary layer (IBL) development is small; for water–land advection IBL development is included [see section 4b(1)(ii)]. We are not accounting for synoptic-scale gradients and advection with this term.

Without advection a positive day-to-day trend in modeled surface and atmospheric temperatures develops as the longwave escaping at the top of the model domain fails to equal the solar radiation absorbed at the surface. This imbalance in the radiative boundary conditions is partly the result of initializing the boundary layer above the relatively extreme (''infinite'') urban surface with a rural sounding. However, similar positive trends are observed, for example at the Spalenring site in Basel, Switzerland, during the Basel Urban Boundary Layer Experiment (BUBBLE) intensive observation period (http://pages.unibas.ch/geo/mcr/Projects/BUBBLE/docs/weather_bulletin.pdf), and may be expected to occur during consecutive sunny days following a cooler period.

3. Model evaluation and sensitivity

Each individual parameterization described in section 2 and used in the combined model has been evaluated against multiple datasets and undergone multiple improvements as a result. Nevertheless, it is important to evaluate whether their combination yields sensible results in terms of surface–atmosphere energy exchanges and resulting near-surface thermal environments. Here, the coupled model is evaluated with observations from the Sperrstrasse site (Table 1) in Basel (47.57°N, 7.58°E) during the BUBBLE campaign (Rotach et al. 2005).

TABLE 1. Selected input parameter values for the urban (TEB) and soil–vegetation models.

Parameter	Unit	Basel urban (Sperrstrasse)	Chicago downtown (LaSalle)	Chicago residential (Norridge)
Geometric parameters				
Building plan area fraction (λ_p)	—	0.54	0.53	0.33
Mean building height	m	14.6	90	7.5
Complete-to-plan area ratio	—	1.92	3.65	2.23
Mean canyon aspect ratio	—	1.00	2.81	0.92
Roof thickness	m	0.092	0.085	0.085
Wall thickness	m	0.131	0.288	0.146
Aerodynamic parameters				
Town roughness length	m	0.88	6.9	0.78
Displacement height	m	9.7	60.0	5.0
Roof roughness length	m	0.15	0.15	0.15
Road roughness length	m	0.05	0.05	0.05
Radiative parameters				
Roof albedo (α_{roof})	—	0.11	0.06 (base)	0.06 (base)
Wall albedo	—	0.25	0.31	0.31
Road albedo	—	0.08	0.15	0.15
Roof emissivity	—	0.91	0.90	0.90
Wall emissivity	—	0.86	0.83	0.83
Road emissivity	—	0.95	0.91	0.91
Thermal parameters*				
Roof layer heat capacities per unit area ($c\Delta x$)	MJ m^{-2} K^{-1}	0.017, 0.005, 0.008, 0.070	0.004, 0.011, 0.001, 0.002	0.004, 0.011, 0.001, 0.002
Wall layer heat capacities per unit area ($c\Delta x$)	MJ m^{-2} K^{-1}	0.014, 0.054, 0.134, 0.028	0.046, 0.241, 0.091, 0.048	0.024, 0.122, 0.046, 0.025
Road layer heat capacities per unit area ($c\Delta x$)	MJ m^{-2} K^{-1}	0.019, 0.078, 0.039, 1.316	0.019, 0.078, 0.128, 1.280	0.019, 0.078, 0.128, 1.280
Roof layer thermal conductivities	W m^{-1} K^{-1}	0.61, 0.13, 0.09, 0.98	0.010, 0.010, 0.060, 0.026	0.010, 0.010, 0.060, 0.026
Wall layer thermal conductivities	W m^{-1} K^{-1}	1.07, 1.08, 1.07, 0.65	3.404, 1.896, 1.920, 1.159	3.404, 1.896, 1.920, 1.159
Road layer thermal conductivities	W m^{-1} K^{-1}	0.75, 0.75, 0.93, 0.28	0.745, 0.745, 0.251, 0.251	0.745, 0.745, 0.251, 0.251
Temperature initialization				
Building interior temperature	°C	19.0	22.0 (summer), 19.0 (winter)	22.0 (summer), 19.0 (winter)
Deep soil temperature	°C	12.0	15.0 (summer), 5.5 (winter)	15.0 (summer), 5.5 (winter)
Natural area		Rural	Urban	—
Natural fraction		1.00	0.16	0.00	0.44
Albedo	—	0.21	0.20	—	0.24
Roughness length	m	0.1	0.5	—	0.45
Wilting point	m^3 m^{-3}	0.12		—	0.114
Soil layer depths	m	0.02, 0.08, 0.95		—	0.02, 0.08, 0.95
Initial soil moisture	m^3 m^{-3}	0.19, 0.22, 0.25	0.28, 0.29, 0.30	—	Surface: 0.21 (summer), 0.16 (spring), 0.11 (winter) Subsurface: 0.30 (summer), 0.23 (spring), 0.15 (winter)

* Thermal parameters are listed in order from the surface layer through to the interior layer.

a. Simulation setup

Roof surfaces are clay tile and gravel over coal tar, wall surfaces are concrete, glass, and brick, and roads are asphalt. Christen and Vogt (2004) provide an estimate for local-scale anthropogenic heat flux at this site of 20 W m^{-2}, neglecting temporal variation. To include hourly anthropogenic heating we use the diurnal variation for Chicago from Sailor and Lu (2004) and adjust its magnitude so as to remain consistent with the mean value of 20 W m^{-2}.

A 48-h clear-sky period beginning at 0000 local solar time (LST) 30 May 2002 is used for the evaluation. Initial profiles of temperature, mixing ratio, and wind speed are provided by a sounding from Payerne airport

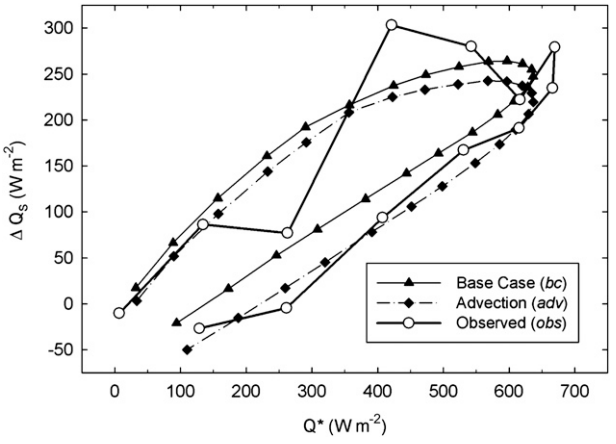

FIG. 1. The obs, bc, and adv storage heat flux vs net radiation. Observed values are residuals of the energy balance. Observations and modeled values are for 0600–1800 LST and are 2-day averages.

TABLE 2. Performance statistics of the combined model for 31-m fluxes and air temperatures during the daytime ($n = 26$ for Q_H; $n = 18$ for Q_E; $n = 146$ for Q^*; $n = 73$ for T_{air}, where n is the number of model–observation pairs). All values are daytime averages over 2 days with the exception of T_{air} (1 day). The units of Q^*, Q_H, and Q_E are watts per meter squared per kelvin, and those of T_{air} are degrees Celsius.

		Q^*	Q_H	Q_E	T_{air}
Bc	Model	415.3	219.6	27.5	20.9
	MBE	−13.6	+15.9	−25.3	+2.0
	RMSE	37.8	57.8	32.5	2.1
	$RMSE_s$	26.7	16.4	31.5	2.1
	$RMSE_u$	26.7	55.4	8.1	0.4
Adv	Model	418.7	242.5	29.0	17.9
	MBE	−10.2	+38.7	−23.8	−0.2
	RMSE	36.0	66.9	30.1	0.6
	$RMSE_s$	26.9	38.7	29.1	0.4
	$RMSE_u$	23.8	54.5	7.6	0.4

(LSMP), Switzerland (46.82°N, 6.95°E) at 0000 LST 30 May 2002. Temperatures in the lower 2 km of the sounding are corrected assuming a 6 K km^{-1} lapse rate to account for the LSMP–Basel elevation difference. Initial surface temperatures are determined using an iterative process where the model is run over the 2-day period and the trend in surface temperature at 0000 LST on the two subsequent days is extrapolated back to the start time, followed by another model run and extrapolation, and so on, until the change between runs becomes insignificant.

A rural simulation is performed using initial soil moisture as a tuning parameter to obtain low-level temperature and flux results that are in good agreement with rural observations at the Grenzach and Village Neuf measurement sites near Basel (Rotach et al. 2005). The intent of these simulations is not to model the rural energy balance but to obtain realistic rural boundary layer profiles for advection. The original [base case (bc)] urban simulation is subsequently rerun with advection from the rural profiles of temperature and mixing ratio (adv simulation), as described in section 2d. In all simulations, temperature and mixing ratio are constantly relaxed toward the 0000 LST 1 June 2002 LSMP sounding profile with $\tau = 1$ day in the free atmosphere (i.e., above the mixed or residual layer) and $\tau = 10$ days below to account for diabatic heating and synoptic- and mesoscale advection; surface layer results were found to be insensitive to the nature of the transition at the boundary layer top between the two relaxation time constants (e.g., step versus gradual change).

Mean bias error (MBE) and root-mean-square error (RMSE) are computed for net radiation (Q^*), sensible heat flux (Q_H), latent heat flux (Q_E), and air temperature (T_{air}) at 31 m. Additionally, RMSE is split into its systematic ($RMSE_S$) and unsystematic ($RMSE_U$) parts. The former may be addressed through better parameter specification, while the latter is a measure of potential model accuracy (Willmott 1982).

A comparison of the coupled model versus TEB-only (offline) sensitivity of canopy air temperature and flux partitioning to roof albedo is conducted starting from the bc and adv simulations; the 0.16 vegetation fraction is converted to road and TEB's sensitivity is examined independent of the soil–vegetation scheme and any surface moisture. The impacts on canyon air temperature (T_{can}), maximum Q^*, and sensible–storage heat flux partitioning (i.e., $\Delta Q_S/Q^* = 1 - Q_H/Q^*$, since $Q_E = 0$) are examined. Subsequently, these simulations are rerun offline, or without feedback from the atmosphere (i.e., without OSU and RS79). Atmospheric output from the lowest OSU model level in the original coupled bc and adv simulations is saved and used as atmospheric forcing for each corresponding offline run, mimicking the use of observed tower data to force TEB. This permits comparison of parameter sensitivity between offline and fully coupled simulations.

b. Evaluation

The model captures the majority of the variation of the net radiation and storage/turbulent partitioning in both the bc and adv simulations (Fig. 1; Table 2). The partitioning of the turbulent flux shows less agreement. Modeled Q_E is about half of the observed value while modeled Q_H is overestimated by a similar absolute magnitude in the bc, suggesting the latent heat flux from the soil–vegetation model is too small (Table 2; Fig. 2). There are many possible explanations, including the neglect of horizontal micro-advection (e.g., the "oasis effect"

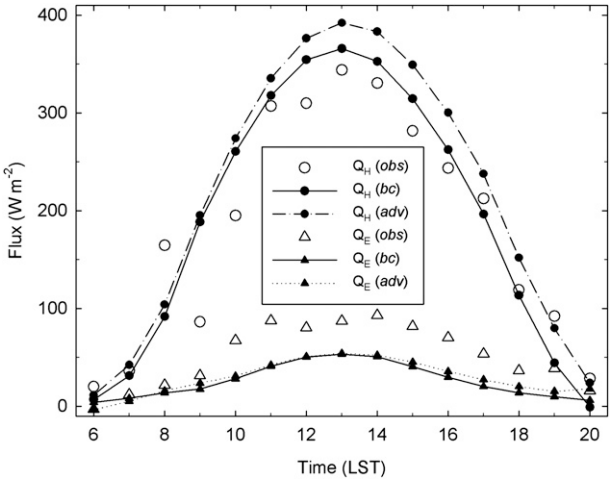

FIG. 2. The obs, bc, and adv 2-day average daytime sensible and latent heat fluxes. Some observed values are missing and are generated by linear interpolation.

at the microscale) and anthropogenic Q_E in the model, and underestimation of the vegetation fraction or the soil moisture. Indeed, the observed latent fraction of the turbulent heat flux [i.e., $Q_E/(Q_E + Q_H) = 0.25$] is larger than the ''natural'' fraction of 0.16, suggesting that at least one of these factors plays a role. The RMSE_S and RMSE_U values in Table 2 indicate that most of the model–observation disagreement in Q_H results from unsystematic variation in the observations; Q_E and T_{air} have larger systematic than unsystematic differences. No attempt was made to weight model input parameters by prevailing wind direction and thus unsystematic disagreement may result partly from the use of model parameters representative of the area surrounding the tower but not necessarily of the source areas influencing the observations.

The inclusion of boundary layer advection from the rural simulation ''brings'' cooler, moister air over the city but does not significantly improve the Q_H/Q_E partitioning for the same reasons as in the base case. However, boundary layer advection mostly removes the air temperature bias and reduces RMSE (the systematic portion in particular). Observations show a clear diurnal oscillation of near-surface wind direction and speed during this period (not shown) suggesting that along-valley slope flows dominate the near-surface wind regime, and therefore that advection plays a substantial role in the urban energy balance. Basel is relatively small in horizontal extent, and thus full boundary layer adjustment to urban surface properties is unlikely to occur. Overall, the evaluation demonstrates that the model substantially captures the variation of energetic processes in the urban atmosphere and resulting thermal climates.

c. Sensitivity

For small roof albedo change (+0.10), sensitivities of maximum Q^* and particularly daytime $\Delta Q_S/Q^*$ with atmospheric coupling are reduced in magnitude relative to their offline values, as expected (Table 3). Sensitivity to a large change in roof albedo (+0.50) permits better differentiation between coupled and offline results in light of the tests of large roof albedo changes to be conducted in section 4. Differences in net radiation sensitivity are small as altered surface–atmosphere radiative exchanges in the coupled model offset each other. However, the daytime storage–turbulent flux partitioning is significantly modified because the offline atmosphere (T_{air} forcing) heats up as though no albedo modification had occurred and erroneously dampens Q_H in favor of ΔQ_S. This highlights the importance of surface–atmosphere model coupling for impact studies, in agreement with Pitman (1994). The effect on modeled canyon air temperature (T_{can}) for both bc and adv is also examined. The former assumes a stagnant atmosphere and could be interpreted as a maximum impact for this scenario, while the latter may be more realistic. Canyon temperature sensitivity is zero in the offline simulations because roof albedo only affects the canyon energy balance in TEB via the boundary layer model (i.e., in coupled mode).

4. Model application: Atmospheric sensitivity to roof albedo

Chicago has recently been a focal point for municipal debates on the implementation of cool roofing technologies for urban heat mitigation (Gartland 2008). Hence, the coupled model is applied to study roof albedo impacts on near-surface air temperatures for two neighborhoods in this city (Table 1): a dense downtown neighborhood (Urban Climate Zone 1; Oke 2006) and a detached residential neighborhood (Urban Climate Zone 3).

a. Simulation design

Initial roof albedo (α_r) is 0.06 in both neighborhoods. We test the impacts resulting from α_r of 0.25, 0.32, and 0.65. These albedos are taken from the U.S. Environmental Protection Agency's Energy Star Program, the 2001 proposed revision to the City of Chicago Energy Code, and subsequent compromises with the roofing industry (Dupuis and Graham 2005; Gartland 2008), and represent a standard gravel–asphalt roof (0.06), gravel–asphalt roofs with lighter-colored aggregate (0.25, 0.32), and a high-reflectivity roof membrane (0.65). Simulations are conducted for clear-sky conditions in three seasons: a hot summer period (with and without a daytime lake

TABLE 3. Sensitivity analysis of varying TEB parameters from the reference bc and the reference adv. Boldface rows are forced by the reference atmosphere (i.e., offline); all remaining rows interact with the model atmosphere. Values are 2-day averages.

	Max Q^* (W m^{-2})	Daytime $\Delta Q_S/Q^*$	Max T_{can} (°C)	Mean daytime T_{can} (°C)
Reference (bc):	636	0.46	27.2	22.5
Roof albedo +0.10	−37	+0.01	−0.7	−0.5
Roof albedo +0.10 offline	**−40**	**+0.02**	**0.0**	**0.0**
Roof albedo +0.50	−187	+0.06	−3.7	−2.8
Roof albedo +0.50 offline	**−201**	**+0.17**	**0.0**	**0.0**
Reference (*adv*):	637	0.39	22.8	19.1
Roof albedo +0.50 (adv)	−183	+0.10	−0.6	−0.7
Roof albedo +0.50 (adv) offline	**−198**	**+0.13**	**0.0**	**0.0**

breeze), a warm winter/spring period, and a very cold winter period. The modeling tests performed are directed toward obtaining the maximum potential impact on urban air temperature. We then represent weather variability in a simple manner to extend the results to seasonal and annual averages.

1) CLEAR SKY

Each clear-sky modeled case consists of a 2-day simulation that begins with an observed sounding of atmospheric temperature, humidity, and wind speed representative of clear weather conditions for the season under consideration (summer, spring, winter). Clear skies are assumed throughout the simulation, maximizing the impact of solar radiation on the surface-layer climate. The impact is further enhanced by assuming a relatively clean atmosphere that allows a maximum amount of direct solar radiation through the atmosphere, no aerosol warming, and only indirect anthropogenic heat resulting from building space heating. These assumptions serve to increase the relative importance of solar radiation absorption by roof surfaces to atmospheric warming. Three of the four simulations are conducted assuming no advective influences on the 1D boundary layer to assess the maximum impacts of roof albedo change on the atmosphere. One additional urban simulation is performed that includes an estimate of cooling due to lake-breeze advection, given Chicago's proximity to Lake Michigan.

2) SEASONAL AND ANNUAL INTEGRATION

To provide seasonal and annual estimates of the average impact on near-surface temperature of roof albedo modifications, some account needs to be taken of the likelihood of clear weather. Our approach is to represent the overall effect of clouds through the use of solar radiation measurements rather than cloud measurements, which themselves are more complex. Observations of solar radiation at the surface integrate the effects of clouds and solar angle, such that their combined impact can be represented by one simple measure: the fraction of clear-sky solar radiation arriving at the surface. Details of the method used are in the appendix.

The residential study area is chosen for this seasonal assessment, as it better represents the most prevalent surface cover in the Chicago area. Simulations are run for three dates: 21 July, representing the period 21 April–20 August (''summer''); 21 March, representing the periods 21 February–20 April (''spring'') and 21 August–20 October (''fall''); and 21 January, representing the period 21 October–20 February (''winter''). These times are selected on the basis of the annual progression of extraterrestrial solar radiation and are intended to provide a minimum number of simulations to assess the seasonal variability. During the winter period, we assume that the vegetated portion of the urban area is snow covered ($\alpha = 0.65$), but that streets and roofs are snow free. The potential seasonal impacts of rooftop snow are estimated by assuming that atmospheric temperature is unaffected by α_r for the periods 21 December–20 February (short snow season) or 1 December–31 March (long snow season) in the seasonal and annual assessments. Results are compared using day 2 of the simulation to allow the model to equilibrate during day 1 of the simulation. No advection is incorporated in this seasonal and annual assessment.

b. Results

1) SINGLE-DAY CLEAR-SKY RESULTS

(i) Overall albedo change

The overall change in neighborhood albedo (α_N), the albedo of the complete urban surface, is shown in Table 4. These values are time-averaged ratios of upward–downward solar radiation output from TEB, and represent snow-free conditions. Typical urban albedos suggested by Oke (1988) are 0.14 for urban centers (range 0.09–0.23) and 0.15 for residential areas (range 0.11–0.24). Therefore, the base case α_N values are somewhat lower in these simulations, especially for the downtown case. The change

TABLE 4. Overall neighborhood albedo as output from TEB for each of the Chicago neighborhoods (snow-free conditions), as well as the input (fixed) urban surface component albedos.

	Neighborhood albedo (α_N)	
Roof	Downtown	Residential
0.06	0.056	0.138
0.25	0.157	0.202
0.32	0.195	0.225
0.65	0.370	0.336
	Surface component albedos	
Vegetation	Street	Walls
0.24	0.15	0.31

to α_N from the increase in α_r to 0.65 is large: from 0.056 to 0.37 in the downtown area, and 0.138 to 0.336 in the residential area. These changes are large relative to typical urban–rural albedo differences of 0.05 or less (Oke 1988). Therefore, the surface modifications considered here represent large intentional climate forcings that are outside of the range of normally observed conditions.

(ii) Summer simulations

The impacts of roof albedo changes are expected to be most important during summer when high solar elevation angles mean that roofs are important for solar radiation interception. The effect of changing α_r in the downtown area has a relatively large impact on the simulations without advection (Fig. 3). The roofs in this area are assumed to occupy over half (53%) of the land surface—a very high fraction likely only realistic for very limited portions of the city.

The largest temperature differences resulting from albedo changes occur in daytime, especially affecting the maximum temperature, while differences are smaller at night. Differences increase from day 1 to day 2 because there is an accumulation of heat in the atmosphere from the urban surface in the low-albedo simulations (0.06–0.32), whereas for the high-albedo (0.65) simulations there is insufficient net available energy at the surface to maintain the input model temperature profile, leading to a cooling of the air over time. In the real atmosphere, some of this difference is offset by the addition/removal of heat via advection.

There are two caveats to note here. First, while TEB has been compared against observations from several neighborhoods in different cities, it has not been evaluated for a dense North American downtown core. Second, the mid-canyon grid point is assumed to be at half the building height. In such deep canyons, there are likely to be further differences between this height and the street-level (i.e., ~2 m) climate that are not explicitly resolved by this model. Changes to roof characteristics may be less influential on the street-level climate within these deep street canyons than the impacts of local shading, for example.

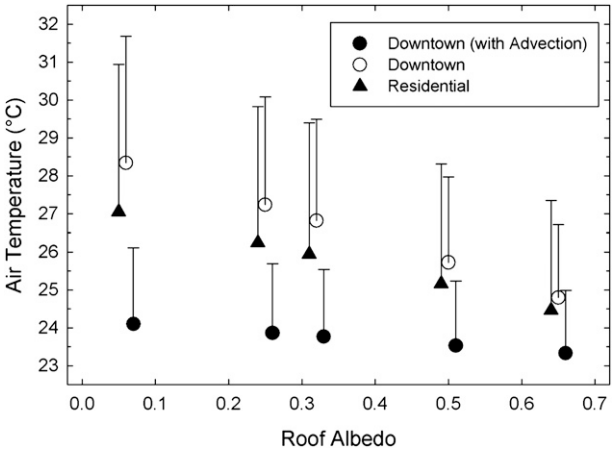

FIG. 3. Summer clear-sky daily average (symbols) and maximum (represented by bars) air temperatures for roof albedo simulations conducted in the downtown (with and without lake-breeze advection) and residential areas. Symbols are offset by up to 0.01 albedo units to prevent plotting over of symbols and error bars.

In the downtown simulation with a modeled breeze from Lake Michigan, the impacts of α_r are reduced substantially: about 80% for the average and maximum temperatures as evidenced by the slopes of the plotted points and error bar tops, respectively, in Fig. 3. The magnitude of these impacts on temperature due to albedo increase is similar to that modeled for winter. The lake breeze is modeled as in section 2d except with a profile of $U(z)$ chosen to mimic the mesoscale lake-breeze phenomenon. Throughout the day $U(z)$ varies sinusoidally in terms of its intensity and the height of its peak, to a maximum of 5 m s^{-1} at 550 m around 1600 LST. IBL development over the $\Delta x = 1075$ m of warm, rough, urban surface between the lake shore and the downtown core is assumed to negate advection in the equilibrium layer (up to 30 m above mean building height) and to dampen advection up to the IBL height of ≈540 m. The advected profile is a summertime rural boundary layer from a nearby sounding with simulated internal boundary layer development over the east–west width of Lake Michigan.

The albedo effects in the residential area are smaller (Fig. 3) because of the smaller building area fraction (0.33). A vegetated fraction of 0.44 partitions some available energy at the surface into evaporative heat flux, and may be expected to increase the effect of roof albedo change relative to the fractional roof coverage because the roof is rendered a more important source of sensible heat in relative terms. Indeed, the sensitivity of temperature to changes in the overall neighborhood albedo (α_N) is slightly larger than for the downtown simulation.

TABLE 5. Change in the 15-m air temperature (°C) arising from the implementation of roof albedo changes from 0.06 to 0.65, 0.06 to 0.32, and 0.06 to 0.25 in the residential area. Results are averaged by season and annually; summer represents the period 21 Apr–20 Aug, spring/autumn represent the periods 21 Feb–20 Apr and 21 Aug–20 Oct, and winter represents the period 21 Oct–20 Feb. Seasonally and annually averaged results and results assuming SCR are shown separately for short (S; 21 Dec–20 Feb) and long (L; 1 Dec–31 Mar) snow seasons. Results from the summer season single clear day are included for comparison.

Parameter	Annual	Annual SCR		Summer	Spring/autumn	Winter	Winter SCR		Clear summer day
0.06–0.65		S	L				S	L	
ΔT_{max}	−1.57	−1.45	−1.28	−2.39	−1.64	−0.68	−0.32	−0.21	−3.59
ΔT_{avg}	−1.05	−0.97	−0.84	−1.64	−1.07	−0.46	−0.21	−0.14	−2.62
ΔT_{min}	−0.54	−0.49	−0.45	−0.98	−0.39	−0.24	−0.11	−0.07	−1.71
0.06–0.32									
ΔT_{max}	−0.65	−0.60	−0.53	−0.98	−0.68	−0.29	−0.13	−0.09	−1.54
ΔT_{avg}	−0.43	−0.40	−0.34	−0.67	−0.44	−0.19	−0.09	−0.06	−1.12
ΔT_{min}	−0.22	−0.21	−0.19	−0.41	−0.16	−0.10	−0.05	−0.03	−0.73
0.06–0.25									
ΔT_{max}	−0.47	−0.43	−0.38	−0.71	−0.49	−0.21	−0.10	−0.07	−1.12
ΔT_{avg}	−0.31	−0.29	−0.25	−0.48	−0.32	−0.14	−0.07	−0.04	−0.82
ΔT_{min}	−0.16	−0.15	−0.14	−0.29	−0.12	−0.08	−0.04	−0.02	−0.53

(iii) Winter and spring simulations

Small α_r changes in either neighborhood result in small changes in the near-surface air temperature for a clear-sky day (typically less than 0.5°C; not shown). The maximum change in α_r (+0.59) yields wintertime temperature decreases of ~1.5°C in the residential area and slightly greater decreases downtown. Slightly larger differences result from the spring simulation.

2) CLOUD AND SEASONAL INTEGRATION

On an annual basis, the impact of the full albedo implementation (0.06–0.65 for all roof area) results in a decrease in the average daily air temperature of approximately 1°C for the residential area (Table 5). An increase of α_r from 0.06 to 0.25 yields an annual decrease of 0.3°C. On a seasonal basis, the impacts are largest in the summer. Decreases in the summertime average daily maximum, average, and minimum temperatures are approximately 60% of those for an individual clear day. In winter, snow-covered roofs (SCR) reduce the average annual cooling by approximately 0.2°C for the long snow season with a smaller reduction for the short snow season (Table 5). Winter season temperature reductions are roughly half and one-third for the long and short periods respectively. All results in Table 5 are considered high estimates of air temperature sensitivity to α_r due to the neglect of advection.

3) CDD/HDD ANALYSIS

Using observed data from Midway Airport and the modeled results from above, an assessment is made of the impact of the altered α_r on the cooling degree-days and heating degree-days for Chicago. Midway Airport is embedded in a more urbanized setting than O'Hare Airport and is characterized by a higher number of CDD and fewer HDD (Table 6). The ratio of HDD/CDD is large in Chicago: 7.8 and 6.1 for O'Hare and Midway Airports' climate normal data respectively. This highlights the relative importance of the winter heating season in Chicago. The difference between O'Hare and Midway is presumably in part due to local differences in degree of urbanization—the Midway region benefits from a reduction in HDD (−415) but requires more cooling (+171 CDD).

Modeled CDD and HDD results use equations derived for each seasonal period from section 4a(2) for the daily average temperature. The results (Table 6) apply to the residential area and do not incorporate advection. Over the 15-yr period for which modeled and observed data can be directly compared, the full albedo implementation yields a decrease of 302 CDD and an increase of 392 HDD. The other implementations also incur a net HDD penalty (i.e., HDD increase is larger than CDD reduction) although the difference is not large. These results assume no rooftop snow in winter. Rooftop snow cover would serve to reduce the impact of α_r in winter and therefore reduce the increase in HDD (i.e., the snow-free simulations overestimate the impact on HDD). Assuming that the roofs remain snow covered for all years of the simulation, the HDD penalty effectively disappears for the short snow cover season; for the long snow season CDD > HDD (Table 6). Advection would act to reduce the magnitude of both HDD and CDD changes.

The frequency of daily CDD from the observations and the modeled air temperatures following implementation of $\alpha_r = 0.65$ in a residential area over the 15-yr period is

TABLE 6. Summary of annual average CDD and HDD changes for uniform implementation of 0.25, 0.32, and 0.65 roof albedos in the residential area. Model simulations are based on temperatures from Midway Airport. HDD with snow represents the impact of snow on roofs for the period 21 Dec–20 Feb (S) and 1 Dec–31 Mar (L). Base 65°F is ≈18°C, and 70°F is ≈21°C.

Method	CDD (base 65°F)	CDD (base 70°F)	HDD (base 65°F)	HDD (base 65°F) with snow	
				S	L
O'Hare Airport: observed (1971–2000)	830	399	6498		
Midway Airport: observed (1971–2000)	1001	515	6083		
Midway Airport: observed (15 yr)	1052	550	5908		
Residential modeled (0.25 roof albedo)	958	479	6021	6004	5978
Residential modeled (0.32 roof albedo)	923	453	6063	6041	6006
Residential modeled (0.65 roof albedo)	750	330	6300	6246	6160
	CDD reduction		HDD increase	HDD increase	
Residential modeled (0.25 roof albedo)	94		113	96	70
Residential modeled (0.32 roof albedo)	129		155	133	98
Residential modeled (0.65 roof albedo)	302		392	338	252

shown in Fig. 4. There is a consistent decrease in daily CDD > 10; for daily CDD < 10, some classes exhibit increases due to the shift in the overall distribution of the values. Decreases of hot days (maximum temperatures greater than 90°F, or ≈32°C) decrease by up to 75% with $\alpha_r = 0.65$; again, these results ignore advection and represent maximum potential impacts.

c. Comparison with other model results

In Table 7 the sensitivity is determined as the ratio of the spatially averaged temperature decrease (ΔT) to the average neighborhood albedo increase ($\Delta\alpha_N$). Maximum daily temperature reductions are used, and every effort is made to match the spatial scales over which the albedo modification and temperature decrease are averaged. Sensitivities are below 12 (i.e., 1.2°C of cooling per 0.10 albedo increase) with few exceptions. In addition to the present results, the three Taha studies are outside of this range. Taha et al. (1988) does not include advection, Taha et al. (1999) includes added vegetation in addition to increased albedo, and Taha (2008) reports maximum local, rather than spatially averaged, cooling; hence, their sensitivities are expected to be somewhat high. The sensitivities in the current study are 18 for the residential area and 16 for the downtown area. These results represent maximum possible impacts for extremely stagnant atmospheric conditions; with lake-breeze advection the sensitivity for the downtown scenario drops to 4, at the lower end of the other studies. Indeed, the median sensitivity of the remaining studies in Table 7 is approximately 5–6, or 0.5°–0.6°C of cooling per 0.10 albedo increase.

The studies in Table 7 include a mix of albedo modifications to roofs, roads, and in some cases, walls. Provided sufficient solar radiation penetrates to the canopy floor, the effect of ground-level albedo modification is expected to more strongly impact the canopy-layer air temperature; recent results from a multilayer canopy scheme yield higher canopy air temperature sensitivity to road albedo (5) than to roof albedo (4) (Hamdi and Schayes 2008; Table 7). Rooftop thermal influence on the canopy is expected to be diluted by boundary layer mixing, an effect that should be better captured with explicit separation of canopy and roof (i.e., with an urban canopy parameterization; e.g., Masson 2000; Kusaka et al. 2001; Martilli et al. 2002). The appropriateness of this latter separation will nevertheless depend on several factors, notably λ_p (flow regime), roof shape, atmospheric stability, and building height variability, or the extent to which a distinct canopy layer exists. The sample of studies in Table 7 with explicit separation of the urban canopy (e.g., Hamdi and Schayes 2008; this study) is too small and varied to draw any conclusions regarding its importance.

Taken together, the studies in Table 7 suggest that $\Delta T/\Delta\alpha_N$ is probably no greater than 1.0°C of cooling per 0.10 increase in α_N, except for extremely stagnant air masses when cooling might reach 1.5–2.0°C (and when the benefits are likely most significant). This is supported by measurements at an idealized desert site that show 0.8°–0.9°C of cooling per 0.10 albedo increase (Rosenfeld et al. 1995; Table 7); however, the absence at this site of a canopy, and of the associated shading, thermal mass, and mixing effects that we expect to decrease the temperature sensitivity to albedo, suggests that it may be a high estimate relative to real cities. A more typical clear-sky summertime sensitivity is probably closer to 0.5°C of cooling per 0.10 increase in α_N. (Furthermore, seasonally averaged results for the Chicago residential neighborhood in Table 7 suggest that temperature sensitivity to albedo for summer, winter, and annual time scales is approximately 65%, 20%, and 45% of the clear-sky value, respectively, assuming no rooftop snow.) Hence, for a moderate (high) density neighborhood with a roof

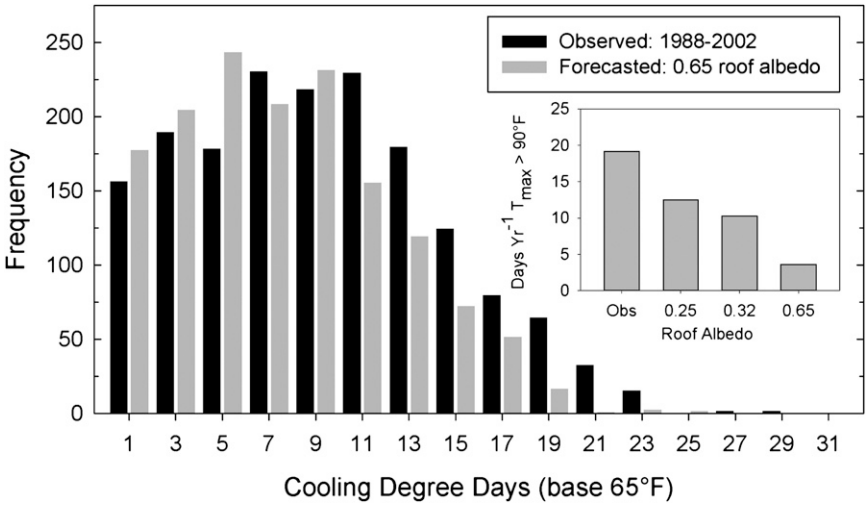

FIG. 4. Change in frequency of cooling degree-days (base 65°F, or ≈18°C) and (inset) number of days per year with $T_{max} > 90$°F (or ≈32°C). Data are from the 15-yr period of 1988–2002 at Midway Airport.

fraction of 0.25 (0.50), uniform α_r increases of 0.40 (0.20) would be required to reduce the air temperature by 0.5°C on a typical clear-sky summer day. The relative merits of such an undertaking from health, comfort, economic, and ecological perspectives are beyond the scope of this paper; furthermore, roof albedo increases have direct and indirect impacts beyond those considered here, such as air pollution mitigation and cooling of the top building floor(s), with attendant effects on health, indoor thermal comfort, and energy use. Importantly, the sensitivity of any particular scenario will depend on a host of factors related to ambient meteorology, season/latitude, geographic setting, and the local character of the urban surface. The range of sensitivity in Table 7 results from a sample of modeling studies with substantial variation in these factors as well as varying degrees of idealization and of spatial and temporal averaging; nevertheless, near-surface air temperature sensitivity to albedo appears to be remarkably constrained.

5. Discussion and conclusions

As applied scientists we seek to evaluate the probable effectiveness of various urban heat mitigation approaches rather than to promote any or all of these approaches. Local-scale in situ urban heat mitigation field experiments have not been undertaken because of cost and logistics, not to mention the difficulty in providing a ''control'' scenario. Hence, modeling approaches are used to quantify the thermal effects of urban surface modification. However, the empirical and theoretical bases for modeling the urban canopy and roughness sublayers remain limited, and our model estimates must be treated with care. At present, several studies of thermal sensitivity to urban surface modification have not explicitly parameterized the urban canopy and roughness sublayer (Taha et al. 1988, 1999; Rosenfeld et al. 1995; Sailor 1995; Sailor and Dietsch 2007; Synnefa et al. 2008; Taha 2008), while others have used schemes with varying degrees of complexity (Krayenhoff et al. 2003; Hamdi and Schayes 2008; this study). Despite recent progress in urban canopy parameterization, *quantification* of the important energetic processes in the urban roughness sublayer lags behind our ability to qualitatively capture these effects (Martilli 2007). Nevertheless, urban canopy parameterization combined with boundary layer or mesoscale modeling is probably the best tool for such quantification given the large range of scales relevant to the urban atmospheric environment (Martilli 2007).

The present work combines several models to represent the most important processes affecting the urban canopy and boundary layer thermal environments. The combined model is evaluated against two days of clear-sky observations from the Basel Sperrstrasse site. The tiled combination of the surface schemes generally compares well with observations, but channels insufficient energy into latent heat. A comparison of offline and coupled surface scheme simulations shows that the latter reduces sensitivity to surface modification because of feedbacks between modeled processes, and is essential for impact studies so that sensitivities of energetic processes to large changes in the surface character are not exaggerated.

On an annual basis, the model simulations show that a change in α_r from 0.06 to 0.65 cools the near-surface air temperature of a Chicago residential neighborhood by about 1°C on average when rooftop snow is included

TABLE 7. Synopsis of studies reporting urban air temperature cooling due to albedo increases; $\Delta\alpha_N$ is average local/neighborhood-scale albedo increase. Cooling is chosen to match the scale of the albedo change and to be the reduction in ≈maximum air temperature during warm (summertime) conditions where possible.

Study	$\Delta\alpha_N$ (difference)	ΔT (cooling)	$\Delta T/\Delta\alpha_N$ (local scale)	Comment
Taha et al. (1988)	0.30	≈9.3°C	31	1D model, no urban canopy-layer scheme; Sacramento, CA
Rosenfeld et al. (1995) modeling	Urban region: 0.13 or urban core: ≈0.30	≈1.5°C (region) or ≈3.0°C (core)	12 or 10	3D mesoscale model, no urban canopy-layer scheme; Los Angeles
Sailor (1995)	Urban region: 0.08 or urban core: 0.14	≈0.6°C (region) or 1.5°C (core)	7 or 11	3D mesoscale model, no urban canopy-layer scheme; roof *and* ground-level albedo increases; Los Angeles
Taha et al. (1999)	Urban region: 0.03–0.05; 0.03–0.04 increase in vegetation too	0.5°–1.5°C (at 1400 LST)	17–30	3D mesoscale model, no urban canopy-layer scheme; albedo change *combined with* vegetation fraction increase
Krayenhoff et al. (2003)	Roofs: 0.45; urban region: 0.05	Region: ≈0.1°C	2	3D mesoscale model Martilli et al. (2002) canopy-layer scheme (partial); roof fraction = 0.10 for entire city (Toronto, Canada); not an extreme summertime case
Synnefa et al. (2008)	Roofs: 0.45 (moderate) or 0.67 (extreme); urban core: 0.23 (moderate) or 0.34 (extreme)[1]	1.3°C or 1.6°C (urban core at 1200–1300 LST)	6 or 5	3D mesoscale model, no urban canopy-layer scheme; Athens, Greece
Hamdi and Schayes (2008)	0.07 (due to 0.16 roof increase);	0.3°C at 1200 UTC (roofs);	4	Offline (no atmospheric model), no advection; Martilli et al. (2002), canopy-layer scheme; 2.5-m within-canopy air temperature; Basel
	0.09 (due to 0.22 road increase)	0.5°C at 1200 UTC (roads)	5	
Taha (2008)	≈0.09 (moderate) or ≈0.17 (high)[2]	Spatially variable; up to 1.0° or 2.0°C locally	≈12 (max local cooling)	3D model, no urban canopy-layer scheme; Southern California
Present study; clear-sky summer day	Roofs: 0.59; neighborhood:			1D model, Masson (2000), canopy-layer scheme with Masson et al. (2002), Lemonsu et al. (2004) updates; Chicago
	0.31 (downtown),	5.0°C	16	
	0.31 (downtown with lake breeze),	1.1°C	4	
	0.20 (residential)	3.6°C	18	
Present study; seasonal, annual	0.20 (residential)	0.7°C (winter)[3]	3	Same as previous
		1.6°C (annual)[3]	8	
		2.4°C (summer)	12	
Sailor and Dietsch (2007); annual	0.20 (for current study residential area)	1.1°–2.1°C (annual)	6–11[4] 3–8[5]	Mitigation Impact Screening Tool (MIST; online) for Environmental Protection Agency; statistical fit to 3D mesoscale model results; Chicago
Rosenfeld et al. (1995) observation	≈0.35	≈3.0°C	9	White Sands National Monument, New Mexico ($\alpha \approx 0.6$) vs surrounding desert ($\alpha \approx 0.26$)

[1] Roof plan area fraction is assumed to be 0.50 for the downtown core of Athens following Martilli et al. (2003).
[2] These values are obtained by taking the average difference over all urban categories from Table 3 in Taha (2008).
[3] Assuming no rooftop snow cover.
[4] Calculated based on modeled temperature range output using input values set to match the 15-yr observed record for Chicago Midway Airport used in the present study.
[5] Range of sensitivities reported for the 20 cities tested using their 3D mesoscale model.

during the winter season. Roof albedo impacts are largest in the summer and smallest in the winter. The impacts are larger in the downtown compared to the residential area because of the larger roof area. During a clear summer day the 0.06–0.65 α_r increase leads to a reduction of about 4°C in the maximum daytime air temperature. Importantly, the size of the albedo increases considered here are well above the range of normally observed variation. Moreover, because of the neglect of advection, all of these temperature reductions are considered to be maximum possible impacts (i.e., typical impacts are expected to be significantly smaller). When an estimate of lake-breeze advection is included, for example, the reduction of the maximum daytime air temperature in the downtown simulation on a clear summer day is reduced by more than half to little more than 1°C.

In the residential area, annual CDD decreases by ≈300 and there are ≈15 fewer days with maximum air temperatures exceeding 90°F (≈32°C) for the simulation period of 1988–2002. There is a net penalty in terms of HDD increase relative to the CDD decrease for all simulations that exclude the effect of snow-covered roofs; the incorporation of a relatively short snow-covered roof season eliminates this penalty. Overall, impacts on HDD and CDD are similar for Chicago according to our analysis, and as such average annual energy use reductions deriving from roof albedo–induced local-scale air temperature reductions are not expected to be significant for this location; net effects for individual buildings may differ. Effects on health and mortality, especially during summer heat waves, may be more significant. Our results suggest that α_r may be effective at reducing the frequency of days with stressful maximum temperatures, although this effect is likely overestimated because of the neglect of advection in the seasonal and CDD/HDD analyses. The impact of larger-scale warming such as that associated with climate change is not included, but would depend substantially on climatological changes to cloud cover. Such larger-scale warming is expected to increase the potential energy and health benefits resulting from decreased CDDs and fewer days with high maximum temperatures. It will also incur a HDD penalty because of a shorter duration of snow-covered rooftops, but this penalty will become less relevant with greater warming.

Near-surface air temperature decreases resulting from α_r enhancement without advection, as modeled in the present study, are consistent with previous work. For studies that include advection, maximum temperature reductions are below 1.2°C per 0.10 increase in average albedo. The present results use a well-evaluated urban canopy parameterization and find sensitivities of ≈1.7°C per 0.10 albedo increase without any advection, dropping to ≈0.4°C with simple estimation of lake-breeze advection. The changes to the overall urban surface albedo considered here are well outside the range of observed values for cities and much larger than urban–rural differences: from 0.056 to 0.370 in the downtown area, and from 0.138 to 0.336 in the residential area. These changes therefore represent a large intentional climate forcing at the local scale. A synthesis of similar results in the literature suggests that a 0.10 average increase in α_N (equivalent to a 0.40 roof albedo increase for a roof area plan fraction of 0.25) will generate a peak daytime air temperature reduction on the order of 0.5°C for typical clear-sky midlatitude summer conditions, while somewhat higher (lower) reductions are likely for more stagnant (advective) atmospheric conditions. The presence of clouds and/or seasonal declines in solar radiation will serve to diminish these impacts. Finally, these estimates of temperature sensitivity to albedo depend heavily on the fidelity of current urban surface–atmosphere exchange models and are expected to be sensitive to meteorological conditions and local urban characteristics.

Acknowledgments. Michael Ek supplied the OSU-CAPS model and associated documentation. Valery Masson provided the TEB model. Ian Harman and Martin Best were helpful in the early stages of the modeling, and Andreas Christen supplied BUBBLE data and documentation. Rene Dupuis provided many of the parameters describing the Chicago neighborhoods and their construction. A significant portion of this work was funded by the National Roofing Contractors Association. ESK acknowledges a postgraduate scholarship and JAV acknowledges research funding support from the Natural Sciences and Engineering Research Council of Canada.

APPENDIX

Seasonal Radiation Modeling for Chicago

To assess the seasonal and climatological variation of solar radiation incident at the surface we use a 15-yr record of total daily observed solar radiation from the Illinois Climate Network, St. Charles station (http://www.sws.uiuc.edu/warm/datatype.asp). For each day, the observed solar receipt is converted to a fraction of the clear-sky value by comparing it to a modeled clear-sky flux obtained from the Bird and Hulstrom (1981) parameterization as described in Iqbal (1983). Results for the entire 15-yr period are shown in Fig. A1a. The frequency distribution indicates that mostly clear cases are the most frequent, with a relatively even distribution from 0.2 to 0.7 and low frequencies of fractions less than 0.2. All fractions greater than 1.0 have been classified as 1.0; this affects 1.3% of the days, most of which (over 80%) are in

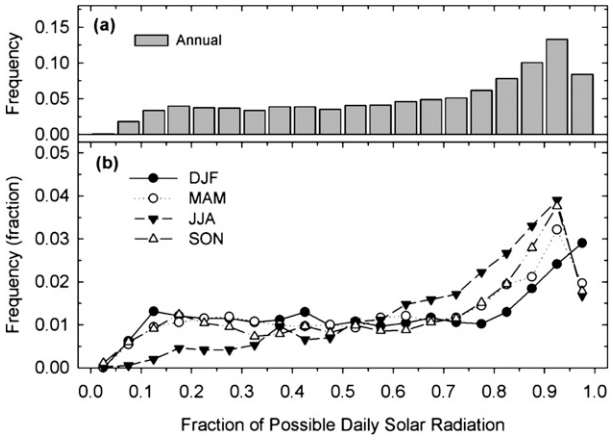

FIG. A1. Frequency distribution of the fraction of clear-sky solar radiation for St. Charles (1988–2002): (a) annual and (b) seasonal distribution.

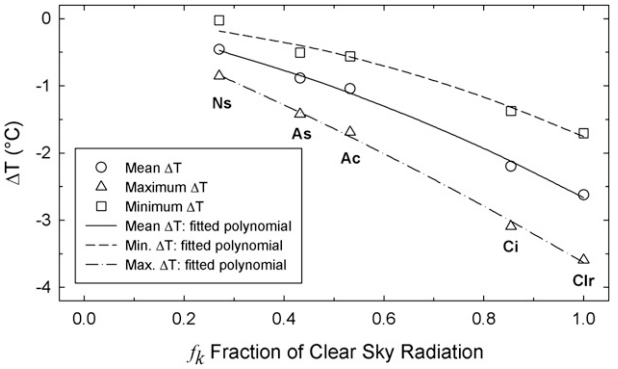

FIG. A2. Modeled temperature differences for 21 Jul due to a roof albedo change from 0.06 to 0.65 for the residential study area with the cloud types listed in Table A1. Results for the day 2 differences in the daily maximum, mean, and minimum temperatures are shown.

the winter when zenith angles are large and total solar radiation is low. On a seasonal basis (Fig. A1b), summer periods are characterized by greater frequencies of relatively clear skies while winter periods have greater frequencies of low fractional solar radiation.

To estimate annual and seasonal impacts of the roof albedo treatments under cloudy conditions, clouds are implemented in the longwave and shortwave radiation schemes (section 2b) and the coupled model is rerun for the residential neighborhood. Because we do not know the exact height, type, or coverage of clouds, we represent four cloud types (Table A1) in the model, each with 100% coverage throughout the simulation period, to provide estimates at four fractional solar radiation levels. The shortwave empirical cloud transmissivity parameterizations of Haurwitz (1948) are used, while climatological cloud thicknesses, heights, liquid water content, and droplet radii required for the longwave scheme are taken from Liou (1992). The cirrus simulation does not include cloud in the longwave scheme because the Roach and Slingo (1979) parameterization does not consider ice, only water droplets. Different amounts of subsidence are used in the various simulations: increasing in strength from January, through March, to July, and increasing in strength with higher pressure synoptic conditions from thick low cloud (Ns: without subsidence) through midlevel (As, Ac) to high-level cloud (Ci) and clear simulations (strong subsidence).

TABLE A1. Modeled cloud types with associated fraction of clear-sky solar and longwave radiation.

Cloud type	Fraction of clear-sky K↓ (integrated over day 2)	Fraction of clear-sky L↓ (integrated over day 2; roof albedo 0.06)
Clear	1.00	1.00
Cirrus	0.85	0.99*
		1.04 (Bolz)
Altocumulus	0.53	1.14
		1.17 (Bolz)
Altostratus	0.43	1.14
		1.2 (Bolz)
Nimbo-/thick stratus	0.27	1.20
		1.24 (Bolz)

* Cirrus fraction of clear-sky L↓ here is cooler because of the reduced solar heating of the ABL over the previous 24 h offsetting the gain in L↓.

The modeled temperature sensitivity as a function of cloud type (i.e., fraction of clear-sky radiation) for the 21 July simulation is shown in Fig. A2. Second-order polynomials are fit to the results with the requirement that the intercept be the origin. This provides equations of the form

$$\Delta T = af_k^2 + bf_k, \tag{A1}$$

which allows the temperature difference for a given α_r increase to be estimated from the fraction of clear-sky radiation (f_k). The coefficients a and b are calculated from simulations for each combination of season and albedo change (e.g., 0.06–0.65). Using polynomials derived from these simulations (e.g., Fig. A2), ΔT is obtained for f_k at intervals of 0.05 and the results are then weighted by the f_k distribution (Fig. A1) to obtain the seasonal and annual estimates of the impact of α_r on air temperature.

REFERENCES

Bird, R., and R. L. Hulstrom, 1981: A simplified clear sky model for direct and diffuse insolation on horizontal surfaces. Solar Energy Research Institute Tech. Rep. SERI/TR-642-761, Golden, CO, 38 pp.

Borden, K. A., and S. L. Cutter, 2008: Spatial patterns of natural hazards mortality in the United States. *Int. J. Health Geogr.,* **7,** 64, doi:10.1186/1476-072X-7-64.

Chang, S., and M. Ek, 1996: Sensitivity study of the CAPS model land-surface scheme using the 1987 Cabauw/PILPS data set. *Phys. Chem. Earth,* **21,** 205–210.

Christen, A., and R. Vogt, 2004: Energy and radiation balance of a central European city. *Int. J. Climatol.,* **24,** 1395–1421.

Clark, P. A., and W. P. Hopwood, 2001: One-dimensional site-specific forecasting of radiation fog. Part II: Impact of site observations. *Meteor. Appl.,* **8,** 287–296.

Dupuis, R. M., and M. S. Graham, 2005: Cooling down Chicago: Chicago's attempt to reduce its heat island results in interesting research findings. *Professional Roofing,* December. [Available online at http://www.professionalroofing.net/article.aspx?id=764.]

Ek, M., and L. Mahrt, 1991: OSU 1-D PBL Model user's guide. Department of Atmospheric Sciences, Oregon State University, Corvallis, OR, 118 pp.

Gartland, L., 2008: *Heat Islands: Understanding and Mitigating Heat in Urban Areas*. Earthscan, 192 pp.

Gueymard, C. A., and D. R. Myers, 2008: Validation and ranking methodologies for solar radiation models. *Modeling Solar Radiation at the Earth's Surface,* V. Badescu, Ed., Springer, 479–510.

Hamdi, R., and G. Schayes, 2008: Sensitivity study of the urban heat island intensity to urban characteristics'. *Int. J. Climatol.,* **28,** 973–982.

Haurwitz, D., 1948: Insolation in relation to cloud type. *J. Meteor.,* **5,** 110–113.

Holtslag, A. A. M., E. I. F. De Bruijn, and H.-L. Pan, 1990: A high resolution air mass transformation model for short-range weather forecasting. *Mon. Wea. Rev.,* **118,** 1561–1575.

Iqbal, M., 1983: *An Introduction to Solar Radiation*. Academic Press, 390 pp.

Krayenhoff, E. S., A. Martilli, B. Bass, and R. B. Stull, 2003: Mesoscale simulation of urban heat mitigation strategies in Toronto, Canada. *Proc. Fifth Int. Conf. on Urban Climate,* Lodz, Poland, International Association for Urban Climate, 343–346.

Kusaka, H., H. Kondo, Y. Kikegawa, and F. Kimura, 2001: A simple single-layer urban canopy model for atmospheric models: Comparison with multi-layer and slab models. *Bound.-Layer Meteor.,* **101,** 329–358.

Lemonsu, A., C. S. B. Grimmond, and V. Masson, 2004: Modeling the surface energy balance of the core of an old Mediterranean city: Marseille. *J. Appl. Meteor.,* **43,** 312–327.

Liou, K. N., 1992: *Radiation and Cloud Processes in the Atmosphere*. Oxford University Press, 487 pp.

Mahrt, L., and H.-L. Pan, 1984: A two-layer model of soil hydrology. *Bound.-Layer Meteor.,* **29,** 1–20.

Martilli, A., 2007: Current research and future challenges in urban mesoscale modelling. *Int. J. Climatol.,* **27,** 1909–1918.

——, A. Clappier, and M. W. Rotach, 2002: An urban surface exchange parameterization for mesoscale models. *Bound.-Layer Meteor.,* **104,** 261–304.

——, Y.-A. Roulet, M. Junier, F. Kirchner, M. W. Rotach, and A. Clappier, 2003: On the impact of urban surface exchange parameterizations on air quality simulations: The Athens case. *Atmos. Environ.,* **37,** 4217–4231.

Masson, V., 2000: A physically-based scheme for the urban energy budget in atmospheric models. *Bound.-Layer Meteor.,* **94,** 357–397.

——, C. S. B. Grimmond, and T. R. Oke, 2002: Evaluation of the Town Energy Balance (TEB) scheme with direct measurements from dry districts in two cities. *J. Appl. Meteor.,* **41,** 1011–1026.

Meehl, G. A., and Coauthors, 2007: Global climate projections. *Climate Change 2007: The Physical Science Basis,* S. Solomon et al., Eds., Cambridge University Press, 748–845.

Oke, T. R., 1982: The energetic basis of the urban heat island. *Quart. J. Roy. Meteor. Soc.,* **108,** 1–24.

——, 1988: The urban energy balance. *Prog. Phys. Geogr.,* **12,** 471–508.

——, 1997: Urban climates and global environmental change. *Applied Climatology,* R. D. Thompson and A. Perry, Eds., Routledge, 273–287.

——, 2006: Towards better scientific communication in urban climate. *Theor. Appl. Climatol.,* **84,** 179–190.

Pan, H. L., and L. Mahrt, 1987: Interaction between soil hydrology and boundary-layer development. *Bound.-Layer Meteor.,* **38,** 185–202.

Pitman, A. J., 1994: Assessing the sensitivity of a land-surface scheme to the parameter values using a single column model. *J. Climate,* **7,** 1856–1869.

Roach, W. T., and A. Slingo, 1979: A high resolution infra-red radiative transfer scheme to study the interaction of radiation with cloud. *Quart. J. Roy. Meteor. Soc.,* **105,** 603–614.

Rosenfeld, A. H., H. Akbari, S. Bretz, B. L. Fishman, D. M. Kurn, D. Sailor, and H. Taha, 1995: Mitigation of urban heat islands: Materials, utility programs, updates. *Energy Build.,* **22,** 255–265.

Rotach, M., and Coauthors, 2005: BUBBLE – An Urban Boundary Layer Meteorology Project. *Theor. Appl. Climatol.,* **81,** 231–261.

Sailor, D. J., 1995: Simulated urban climate response to modifications in surface albedo and vegetative cover. *J. Appl. Meteor.,* **34,** 1694–1704.

——, and L. Lu, 2004: A top-down methodology for determining diurnal and seasonal anthropogenic heating profiles for urban areas. *Atmos. Environ.,* **38,** 2737–2748.

——, and N. Dietsch, 2007: The urban heat island Mitigation Impact Screening Tool (MIST). *Environ. Modell. Software,* **22,** 1529–1541.

Synnefa, A., A. Dandou, M. Santamouris, M. Tombrou, and N. Soulakellis, 2008: On the use of cool materials as a heat island mitigation strategy. *J. Appl. Meteor. Climatol.,* **47,** 2846–2856.

Taha, H., 2008: Urban surface modification as a potential ozone air-quality improvement strategy in California: A mesoscale modeling study. *Bound.-Layer Meteor.,* **127,** 219–239.

——, H. Akbari, A. Rosenfeld, and J. Huang, 1988: Residential cooling loads and the urban heat island—The effects of albedo. *Build. Environ.,* **23,** 271–283.

——, S. Konopacki, and S. Gabersek, 1999: Impacts of large-scale surface modifications on meteorological conditions and energy use: A 10-region modeling study. *Theor. Appl. Climatol.,* **62,** 175–185.

Troen, I. B., and L. Mahrt, 1986: A simple model of the atmospheric boundary layer: Sensitivity to surface evaporation. *Bound.-Layer Meteor.,* **37,** 129–148.

Willmott, C. J., 1982: Some comments on the evaluation of model performance. *Bull. Amer. Meteor. Soc.,* **63,** 1309–1313.